Microscopic structure of $LiCl.6D_2O$ in glassy and liquid phases

1991 J. Phys.: Condens. Matter 3 551

(http://iopscience.iop.org/0953-8984/3/5/005)

J. Phys.: Condens. Matter 3 (1991) 551–567. Printed in the UK

Microscopic structure of $LiCl \cdot 6D_2O$ in glassy and liquid phases

J F Jal†, A K Soper‡, P Carmona† and J Dupuy†

† Département de Physique des Matériaux, UA 172, Université C Bernard, Lyon 1, Villeurbanne, France

‡ Rutherford Appleton Laboratory, Chilton, Didcot, Oxon OX11 0QX, UK

Received 9 August 1990

Abstract. We present the first experimental analysis of the chlorine–water distribution in the glassy and liquid state of $LiCl \cdot 6D_2O$. The results are based on neutron diffraction experiments performed at a spallation source. Evidence of a fundamental structural change within the hydration shell around a chlorine ion in the glassy state is given although the D_2O intramolecular characteristics remain unchanged. At the same time, as the water molecules become more localized within the chlorine hydration shell, the system orders over nearly twice the distance (three more D_2O shells being detectable) and this is possibly accompanied by an ordering of the ion distribution.

1. Introduction

In aqueous solutions, the chlorine ions impose some local ordering and selective dynamical motion on the water molecules. At room temperature, the electrolyte is still in dynamical exchange. By quenching the solution, a glass is formed and its dynamics is greatly reduced. A large number of salts dissolved in water are able to form glassy materials [1]. They are generally accepted as 'fragile' glasses [2], their viscosity not varying with temperature according to an Arrhenius law. Among these salts, LiCl and $BeCl_2$ present the ability to form deeply *supercooled liquids* at particular concentration ranges [3, 4], the onset of crystallization being reduced by slow kinetics.

In the supercooled state the viscosity of such systems is analysed [5] within the framework of the usual scaling theory as a second-order transition. The structural properties at medium and large distances exhibit self-similar behaviour accompanied by the presence of density and concentration fluctuations [2]. These fluctuations are arrested and the scaling behaviour of the structural relaxation stopped at a characteristic temperature T_0 considered as the lowest intrinsic limit of the metastability state. This is also the highest limit for the glass transition which is characterized by strongly time-dependent local structural distortions [2, 5, 6].

It should be possible to explore the existence of a dynamical singularity corresponding to an instability of the liquid phase by exploring the connectivity of the H bond network of an electrolyte. In particular, the behaviour of the medium-range order should be investigated using an H/D substitution [7]. In other words, one can attempt to explore the glass transition by studying supercooled liquid electrolytes.

0953-8984/91/050551 + 17 $03.50

However, before undertaking advanced studies it is necessary to question the extent of the structural differences between a glass and a liquid electrolyte and to test the possibility of precise structural characterizations. To this end, the solution, $LiCl \cdot RD_2O$ is chosen with $R = 6$ (R being the number of moles of D_2O per mole of salt). At this composition the deep metastable eutectic extending well under the glass transition prevents crystallization, and, following the model proposed by Franck and Wen [8], the ions are surrounded by an hydration sphere and there are few chances for direct ion–ion correlations. For this system $T_0 = 145$ K and $T_g \approx 138$ K (as defined in [9]).

$LiCl \cdot RH_2O$ (or its equivalent $LiCl \cdot RD_2O$) is an excellent system in which to investigate the structural short- and medium-range order because isotopic substitution is easy on Li, H and Cl.

Since we assume, and will verify, that intramolecular D_2O structure is unaffected by the thermodynamic state, it is possible to obtain the structural differences between the Li^+ and Cl^- coordination shells in the liquid and glassy state. Due to its more suitable neutronic characteristics the chlorine–water distribution will be investigated first, although a greater effect could be expected for the lithium–water distribution.

In this paper we present the first experimental analysis of the chlorine–water distribution in the glassy and liquid state based on neutron diffraction experiments performed at a spallation source with a Q-range such as to observe differences in the medium-range order.

In the first section we present the experimental procedure with emphasis on details which are typical of time-of-flight measurements. The data analysis is then described in the second section. The measured total intensity has to be corrected for the contribution from the sample environment and from multiple, incoherent and inelastic scattering. The corresponding correction programs are classical and we will simply point out the details of the data analysis that permit us to assert the quality of the measurements. Finally, in the last section we will compare and discuss the structure of the liquid and glassy states.

2. Experimental procedure

2.1. Measurement of the sample total neutron cross section

In the case of light atoms such as hydrogen and deuterium, or molecules containing light atoms, there is no simple energy dependence of the total neutron cross section (σ_T) since, among other things, the inelastic scattering, and consequently the total scattering cross section, varies substantially with the energy of the incident neutron.

It is therefore necessary to obtain the total neutron cross section of the sample in a transmission experiment. Since our sample is cylindrical and narrower than the beam width, we must compare the sample transmission measurement with that of a reference sample with identical positioning and geometry. This requirement is especially important in view of the non-uniformity of the beam profile. A vanadium rod is chosen as a reference. From the known energy dependence of the vanadium cross section [10] it is possible to determine the effective neutron beam width at the sample position. In figure 1(a) we see that the linear wavelength dependence of the vanadium σ_T value is well reproduced for an effective beam width of 1.1 cm. The same width is then used for the sample, but, as shown in figure 1(b), the energy dependence of the $^7LiCl \cdot 6D_2O$ sample cross section is no longer a simple function, since molecules containing light atoms are

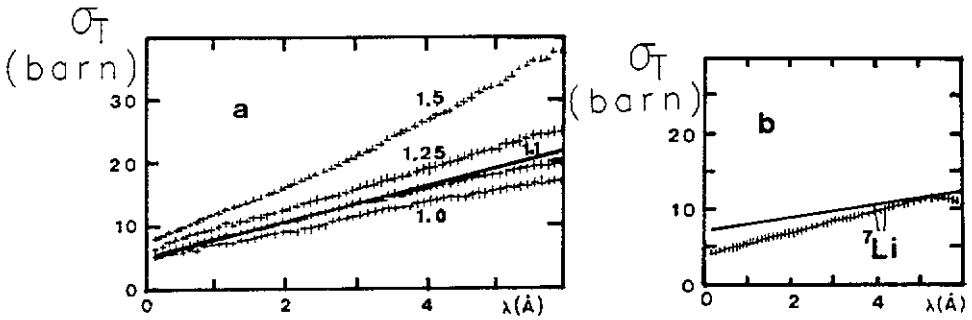

Figure 1. Total cross section σ_T versus wavelength: ———, calculated assuming bound cross section values, (*a*) for vanadium bar with different beam widths, (*b*) for sample with 1.1 beam width; +++, experiment.

now involved. In particular the measured cross section is still well below its bound values at high energies (short wavelengths).

Table 1 gives the characteristics of the samples measured over two periods referred to as experiment 1 and experiment 2. σ_s is the total scattering cross section calculated by the relation

$$\sigma_s = \sigma_{coh} + \sigma_{incoh} = 4\pi b_s^2 \qquad b_s^2 = \sum_\alpha c_\alpha \bar{b}_\alpha^2$$

where c_α is the atomic fraction, b_α the scattering length of the element α, and the bars indicate averaging over the spin and isotopic states of each element.

2.2. *Experimental conditions of the TOF diffraction measurement*

The experiment was performed at ISIS on the LAD spectrometer. The sample, in a vanadium cylindrical container, was quenched immediately after a first quick 'test run'. The temperature reached with a quench rate (QR) of around 3 K min^{-1} was 125 K.

Table 1. Chemical and neutronic characteristics of the sample.

	$^7LiCl \cdot 6D_2O$ Experiment 1	$^7Li^{35}Cl \cdot 6D_2O$ Experiment 2	$^7Li^{37}Cl \cdot 6D_2O$ Experiment 2
Isotopic composition	100% ^7Li 75.8% ^{35}Cl 99.52% D_2O 0.48% H_2O	100% ^7Li 99% ^{35}Cl 99.46% D_2O 0.54% H_2O	100% ^7Li 91% ^{37}Cl 99.52% D_2O 0.48% H_2O
σ_{coh} (b)	4.645	4.799	4.227
σ_{incoh} (b)	1.805	1.774	1.609
σ_s (b)	6.450	6.573	5.836
b_s^2 (b sr^{-1})	0.513	0.523	0.464
σ_a at 1.8 Å	1.678	2.186	0.221
σ_T	8.128	8.759	6.057
Vanadium cell:			
diameter φ (cm)	0.8	0.8	0.8
height h (cm)	4	3	3

Table 2. Neutronic conditions at ISIS during the two measuring periods.

	Experiment 1 July 1987	Experiment 2 January 1988	
Sample	$^{7}LiCl \cdot 6D_2O$	$^{7}Li^{35}Cl \cdot 6D_2O$	$^{7}Li^{37}Cl \cdot 6D_2O$
Average current† (μA)	33	49	
Integrated current per month ($\mu A\ h^{-1}$)	22 000	25 000	
Measuring time at 123 K	12 h 30 min	17 h 30 min	26 h
Measuring time at RT	16 h	15 h 30 min	19 h

† Currents up to 110 μA are now routinely available (1990).

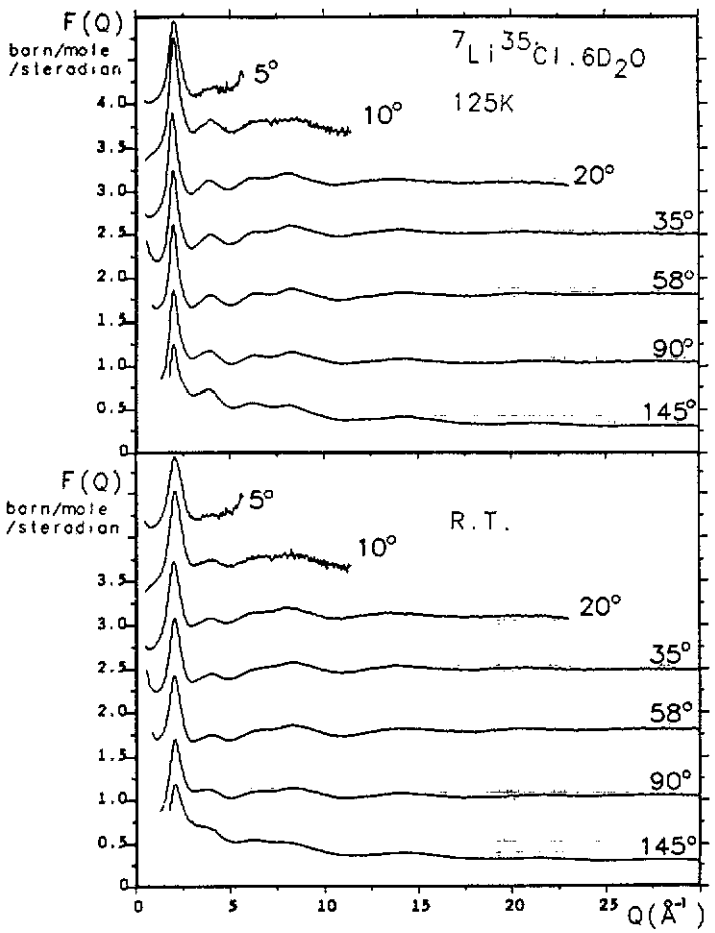

Figure 2. Total structure factor measured at several scattering angles for the same material $^{7}Li^{35}Cl \cdot 6D_2O$ at two temperatures, during the same run.

Table 3. Values of the coefficients of $S_{\alpha\beta}(Q)$ in equation (1).

	Li–Li	Cl–Cl	Li–Cl	Cl–O	Cl–D	Li–O	Li–D	O–O	O–D	D–D
^{35}Cl	0.12	3.37	−1.28	20.2	46.2	−3.83	−8.75	30.33	139	158
^{37}Cl	0.12	0.37	−0.43	6.72	15.4	−3.83	−8.75	30.33	139	158
^{N}Cl	0.12	2.29	−1.05	16.7	38.1	−3.83	−8.75	30.33	139	158

Higher QR is not necessary at this concentration [3]. The neutronic conditions available at ISIS during the two measuring periods are given in table 2.

The room temperature run was performed immediately after the low-temperature one. This procedure reduced the vanadium corrosion to a negligible value.

An illustration of the data obtained for $^{7}Li^{35}Cl \cdot 6D_2O$ at low and room temperatures is given in figure 2 for several scattering angles. These data are corrected for background, multiple, can and cryostat scattering following a standard procedure [11]. We obtained a time of flight (TOF) differential cross section (TDCS) from which it is possible to determine the total structure factor $F(Q)$ which directly describes the structure of the multicomponent system investigated.

The total structure factor is related to the partial structure factors $S_{\alpha\beta}(Q)$ by the relation

$$F(Q) = \sum_{\alpha} c_\alpha \overline{b_\alpha^2} + \sum_{\alpha\beta} c_\alpha b_\alpha c_\beta b_\alpha (S_{\alpha\beta}(Q) - 1) = b_s^2 + \sum_{\alpha\beta} c_\alpha c_\beta b_\alpha b_\beta (S_{\alpha\beta}(Q) - 1) \qquad (1)$$

where c_α is the atomic fraction, b_α the scattering length of element α, and the bars indicate averaging over the spin and isotopic states of each element. The first term comes from 'single-atom' scattering; the second is due to 'interference scattering' and contains the basis structural information on atomic pair positions.

Table 3 gives the value of the coefficients of each $S_{\alpha\beta}$ partial contribution to $F(k)$ for the three chlorine isotopic compositions of the $^{7}LiCl \cdot 6D_2O$ sample studied. These coefficients are independent of the state of the system. Therefore, small errors in the isotopic composition have negligible effect on the temperature dependence of the structural characteristics. However, the density must be known with precision [12].

Table 4. Density and related parameters for the different isotopics compositions.

	$^{7}LiCl \cdot 6D_2O$	$^{7}Li^{-35}Cl \cdot 6D_2O$	$^{7}Li^{-37}Cl \cdot 6D_2O$
d			
130 K	1.289	1.284	1.298
RT	1.264	1.259	1.273
ρ ((atoms) Å^{-3})			
130 K	0.09569	0.09565	0.09564
RT	0.09384	0.09378	0.09380
N_s (atoms)			
130 K	0.1924	0.1442	0.1442
RT	0.1886	0.1414	0.1415
$N_s b_s^2$ (b sr^{-1})			
130 K	0.09870	0.07542	0.06691
RT	0.09675	0.07395	0.06566

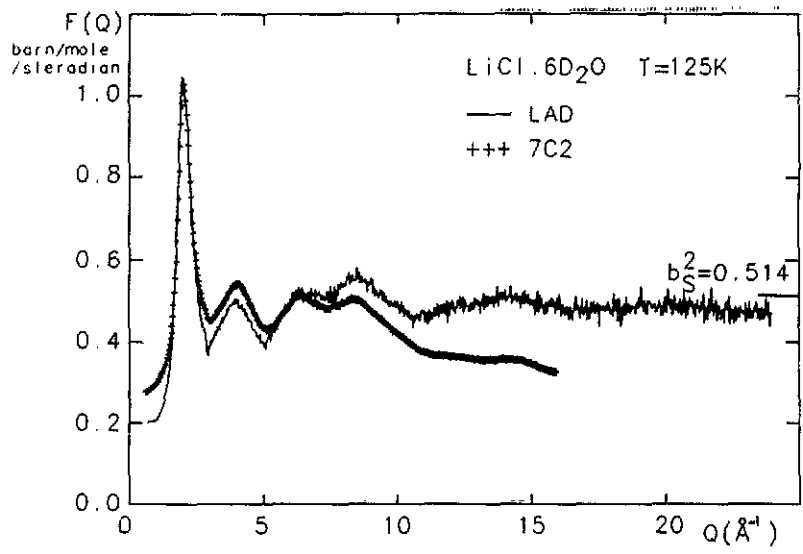

Figure 3. Total scattering intensity for $LiCl \cdot 6D_2O$ at 125 K, before inelasticity corrections measured: ———, on LAD, ISIS (RAL), UK; +++, on 7C2 ORPHÉE (LLB) Saclay, France.

Table 4 gives the density d, the number density ρ, the number of atoms in the beam N_s ($N_s = \pi\varphi^2 h\rho/4$), with h and φ the cell height and internal diameter, and $N_s b_s^2$ the total cross section (divided by 4π).

Before discussing the experimental results, we want to point out some improvements on the data analysis made in order to increase the precision.

3. Data analysis

We will focus our comments on a few points: the inelasticity correction, the sum rule and the comparison between TOF (spallation source) and constant-wavelength (reactor-based) fully corrected data.

3.1. Inelastic correction

In general, neutron diffraction in materials containing light elements such as D and Li is distorted by the inelasticity correction since the quasistatic approximation is not valid. Empirical correction methods have been developed for reactor experiments but they remain to be justified. However, with pulsed neutrons the inelasticity correction is small for D and Li if the detector angle is $\leqslant 40°$.

In figure 3, we give the total scattering intensity in barns per steradian obtained on $LiCl \cdot 6D_2O$ at 125 K in a constant-wavelength measurement (at the ORPHEE reactor, on the 7C2 spectrometer with $\lambda = 0.703$ Å) before making inelasticity corrections. We also display the results obtained on the LAD for a detector angle of $2\theta = 20°$. The fall off, which is characteristic of inelasticity effects on the self-scattering term in reactor data, is nearly absent in TOF measurements. It is also apparent that the intramolecular bonds produce oscillations up to very high values of Q. We note that the high-Q limit of the

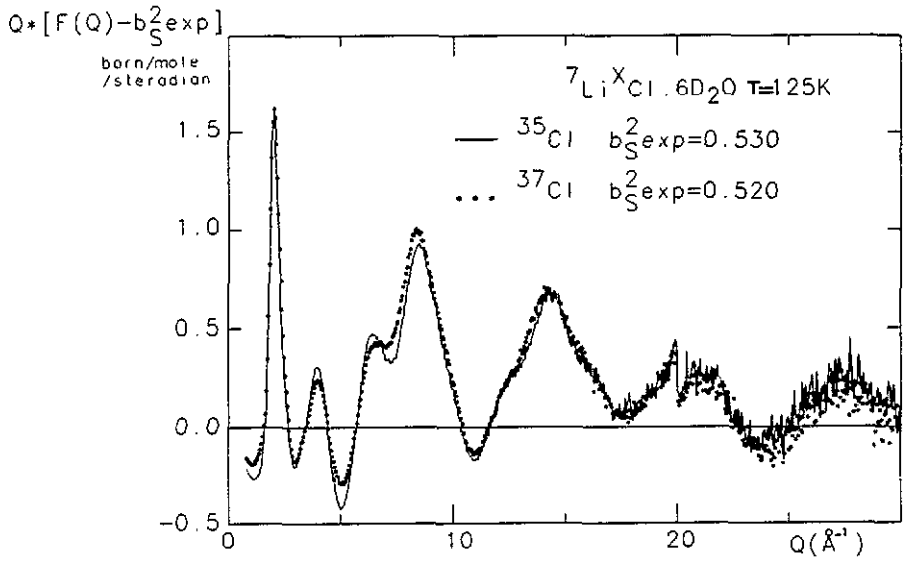

Figure 4. Total structure factor obtained for $^7Li^*Cl \cdot 6D_2O$ for the two isotopic compositions at 125 K: ———, 99% ^{35}Cl, 1% ^{37}Cl; · · ·, 91% ^{37}Cl, 9% ^{35}Cl.

scattering level for the LAD data compares well, within 8%, with the known scattering cross section which gives an overall estimate of the data correction accuracy. The differences observed in the low-Q region are related to the corrections detailed in section 3.2.

3.2. Additional use of maximum entropy

In figure 4, we display $Q(F(Q) - b_s^2)$, b_s^2 being determined experimentally at the high-Q limit. There is a step in the data at 20 $Å^{-1}$: the data shown here have been merged from data taken at separate scattering angles of 5°, 10°, 20° and 35° and the step seen here arises from the difference between the greatest inelasticity 'droop' at 35° and that at 20°.

The measurements obtained with ^{35}Cl and those obtained with ^{37}Cl isotope seem to agree remarkably well. However, the oscillations due to the distinct scattering are not well balanced around zero and the sum rule is not satisfied. A smoothly Q-dependent correction residue is apparent and could be the effect of cumulating errors in the various corrections. Maximum entropy allows us to correct the data for this correction residue. The modified maximum entropy algorithm was developed by Soper [13]. Essentially, the method uses a Monte Carlo (MC) algorithm to explore a range of correlation functions consistent with the data, while at the same time a smoothness constraint is placed on the possible distributions: the smoother distributions are favoured over the noisier distributions. The degree of fit to the data is measured by the R-factor, R_f, where

$$R_f^2 = \sum (D_i - M_i)^2 \Big/ \sum D_i^2. \tag{2}$$

The D_i are the data in question and M_i models the data generated by the MC algorithm.

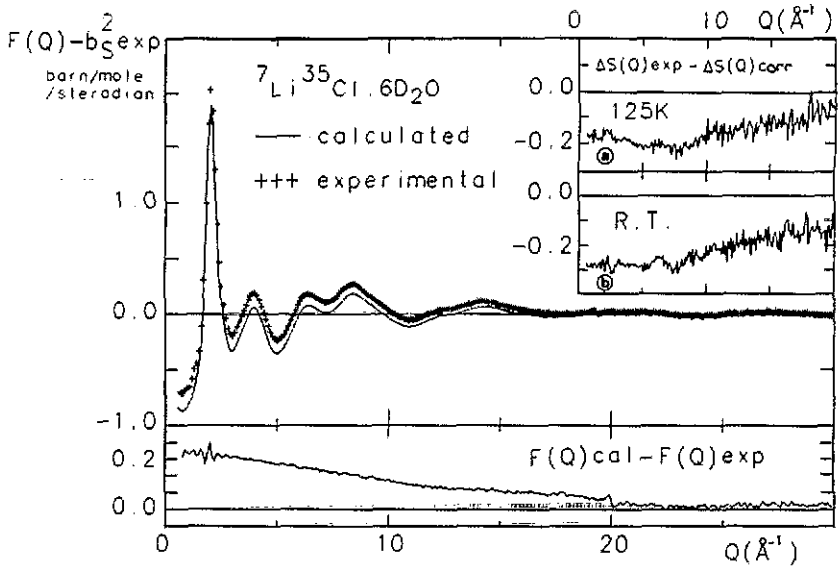

Figure 5. Total scattering cross section corresponding to $^{7}Li^{35}Cl \cdot 6D_2O$ at 125 K: ———, measured; +++, as corrected by maximum entropy—in the bottom of the figure the smoothly correction residue is given. Inset: correction residues of the first-order difference at two temperatures.

The information content of any particular distribution N_j is represented by the function

$$I = |N_j''|^2/|N_j'| \tag{3}$$

which is essentially a function of the second (double prime) and first (single prime) derivatives of N_j. Clearly, as I becomes smaller the distribution becomes smoother. The effect of the first derivative in the denominator is to down-weight the second derivative in regions in which N_j is changing very rapidly, such as in the vicinity of peaks.

These two terms are combined to form a 'quality factor' Q_f, where

$$Q_f = \lambda_1 R_f^2 + \lambda_2 I \tag{4}$$

and λ_1 and λ_2 are undetermined weights that control the fit to the data and the degree of smoothness in the final solution, respectively. The second weighting is chosen in such a way that on average the second term in (4) and the R-factor make equal contributions to the quality factor. At each stage of the algorithm the acceptance of each trial distribution is based on the value of $\exp(-Q_f)$. The distribution presented is therefore the ensemble average of all accepted trial distributions, and because the simulation has sampled a range of distributions consistent with the data and with the degree of smoothness imposed, a realistic standard deviation of individual distributions about the average can be calculated, giving rise to a realistic error bar in the final estimate.

Figure 5 shows, as a full curve, the fully corrected distinct scattering cross section $F(Q) - b_s^2$; the smoothly Q-dependent correction residue is also displayed. The improvement is significant.

No further effort was made to master the correction residue problem, since the present study aimed essentially to make a comparison between two structures. We

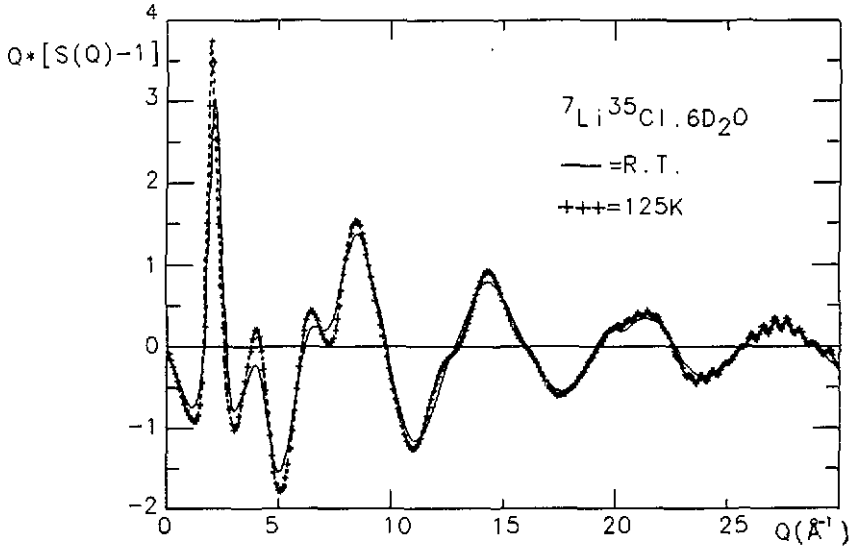

Figure 6. Maximum-entropy structure factor for one isotope composition at two temperatures.

verified, however, that the correction residue was practically independent of isotopic composition and sample temperature.

The differences between the residues $(\Delta S(Q)_{ex} - \Delta S(Q)_{corr})$ of the normalized differential cross sections of the two isotopic compounds in the glassy and liquid states are given in the inset of figure 5. These differences are small and comparable.

To conclude, we consider as acceptable the corrections proposed for similar future studies although there could be more improvement [14]. However, they are small when compared with the advantage of obtaining data on an extended Q-range.

3.3. Comparison with an equivalent study at RT

The groups of G W Neilson and J E Enderby have compared [15] the scaled $F(Q)$ or $\Delta F_{Cl}(Q)$ for three LiCl solutions corresponding respectively to $R = 14$ (dilute), $R = 5$ (the nearest concentration to our study), and $R = 3.35$ values. The agreement between our study and their $R = 5$ data is satisfactory. Nevertheless, they do not observe asymmetry on the second peak, near 3 $Å^{-1}$, on $\Delta F_{Cl}(Q)$ (figure 8), and their data stop before significative structural oscillations can be detected.

4. Results and discussion

4.1. The total structure factor and intramolecular structure of water

The total structure factors measured at two tempertures are given for $^7Li^{35}Cl \cdot 6D_2O$ in figure 6. The total structure factor is defined by relation (3).

$$(S(Q) - 1)\left(\sum_{\alpha} c_\alpha b_\alpha\right)^2 = \sum_{\alpha\beta} c_\alpha c_\beta b_\alpha b_\beta (s_{\alpha\beta}(Q) - 1) \qquad (5)$$

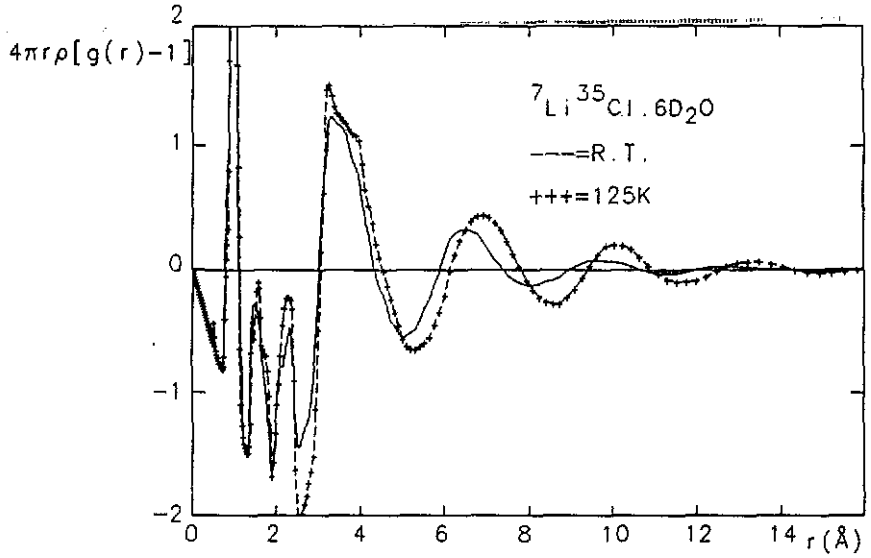

Figure 7. Total pair correlation function $4\pi\rho r(g(r) - 1)$ of $^{7}Li^{35}Cl \cdot 6D_2O$ obtained at RT, ———; and at 125 K, +++.

with, according to equation (1),

$$S(Q) = \left[(F(Q) - b_s^2) \Big/ \left(\sum c_\alpha b_\alpha \right)^2 \right] + 1.$$

Details on the data corrections have been described in the previous section.

The curves exhibit a regular oscillatory behaviour and become nearly identical in the high-Q region: ($Q > 17$ Å^{-1}). We conclude that the intramolecular structure of water remains unaltered. This is confirmed by the examination of the total pair correlation function (see figure 7) where we identify the first two peak positions, with the intramolecular r_{OD}, r_{DD} distances which are equivalent to the pure water intramolecular distances [16] at RT:

$$r(\mathrm{DD}) \approx 1.57\ \text{Å} \qquad r(\mathrm{OD}) \approx 0.97\ \text{Å}.$$

For Q-values less than 17 Å^{-1} we observe some difference between the liquid and the glass phase structures. The differences are detected as a low-Q shift for the first diffraction peak and an improved resolution for all the peaks of the glassy state. This last effect is noticeable even in the range 11 Å^{-1}–17 Å^{-1}, although MD calculations show [14] that, in this range, the oscillations should be mainly due to the intramolecular water structure.

4.2. First-order differences in the liquid and glassy state

The pair correlations between Cl and the various atoms can be obtained from the first-order difference between diffraction patterns measured with different chlorine isotopes

Table 5. The weight of various partial structure factors contributing to the difference $\Delta F_{Cl}(Q)$.

	Cl–D (10^{-3} b sr^{-1})	Cl–O (10^{-3} b sr^{-1})	Cl–Li (10^{-3} b sr^{-1})	Cl–Cl (10^{-3} b sr^{-1})
^{35}Cl–^{37}Cl	13.4	30.8	−0.9	3
^{N}Cl–^{37}Cl	9.88	22.73	−0.58	2

[18]. Table 5 gives the weight of the various partial structure factors contributing to the difference:

$$\Delta F_{Cl}(Q) = F(Q)(^{*}Cl^{7}Li \cdot 6D_2O) - F(Q)(^{**}Cl^{7}Li \cdot 6D_2O)$$

where *Cl and **Cl are two different chlorine isotopic compositions.

Of course, the higher precision on the water molecule–Cl coordination comes from the difference between ^{35}Cl and ^{37}Cl data, which is given in figure (8) for the glassy and liquid states. In this figure, the curves become similar above 17 Å^{-1}, in agreement with the total structure factor characteristics for the two states, but large differences appear at lower Q-values. The first peak of the glassy differential pattern is very narrow and shifted to low Q-values, while the third and fourth peaks are shifted to high Q-values; a shoulder is also noticeable on the left-hand side of the 2nd peak. Between 11 and 17 Å^{-1} all oscillations are in phase and only intensity differences persist. The large Q-range over which the oscillations differ tells us something about an increased ordering within the hydration shell of chlorine in the glassy state, the narrow first peak pointing to correlated large-distance effects.

By comparison, pure water liquid and amorphous states differ only at low Q-values [19].

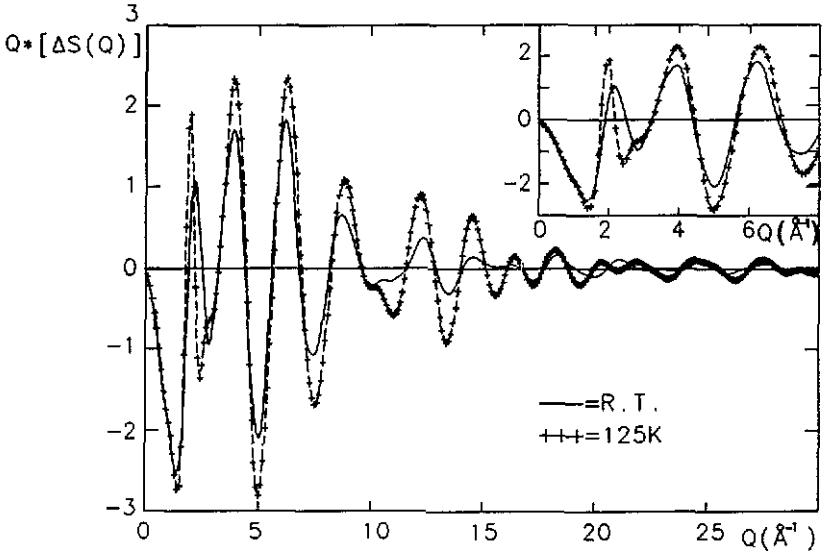

Figure 8. First-order difference between diffraction patterns measured with two isotopic compositions at 125 K, +++; at RT, ———. Inset: magnification of the intermediate Q-range.

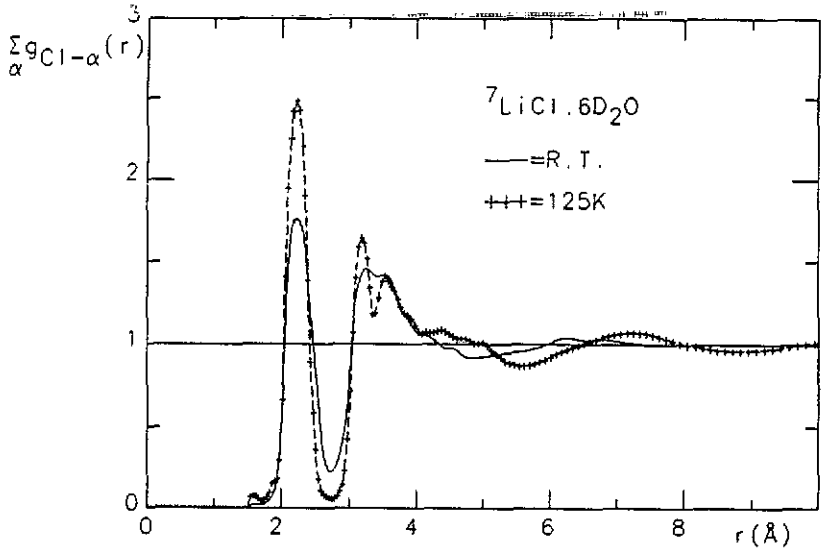

Figure 9. Pair correlation functions $\Sigma_\alpha g_{Cl-\alpha}(r)$: +++, at 125 K; and ———, at RT.

4.3. Pair correlation functions Cl–α (α = O, D, Li, Cl) in the liquid and glassy state

The Fourier transforms of the first-order difference functions measured in the liquid and glassy states are given in figure 9. In this highly concentrated aqueous system we observe, in the vitreous state, a very well defined first peak, $g_{Cl-\alpha}$ which goes to zero at the first minimum. The phase agreement up to 4 Å confirms the stability of the first hydration shell around chlorine in both states.

The weightings of the different Cl–α pair correlation functions participating in the FT of the first-order difference ^{35}Cl–^{37}Cl are:

$$\Delta g(r) = 0.642\, g_{Cl-D}(r) + 0.280\, g_{Cl-O}(r) + 0.1035\, g_{Cl-Cl}(r) - 0.025\, g_{Cl-Li}(r)$$

permits us to attribute the first well defined distance to Cl–D_1. The differentiation between Cl–O and Cl–D_2 is sharp in the glassy state and smeared in the liquid.

The hydration of chlorine is basically unaffected by vitrification but the various atoms become significantly more ordered within the hydration shell.

The first peak positions are given in table 6 with the notation used in [17].

Table 6.

Cl		r_1 (Å) (cut off)	r_{M1} (Å) first maximum distance	$g(r_{M1})$	r_{m1} (Å) first minimum distance	$g(r_{m1})$
D_1	Glass	1.825	2.225	2.67	2.675	0
	Liquid	1.825	2.225	2		0.3
O	Glass	2.7	3.175	1.7	3.2–3.7	1.3
	Liquid	2.7	3.2	1.6		1.5
D_2	Glass		3.625			
	Liquid		3.625			

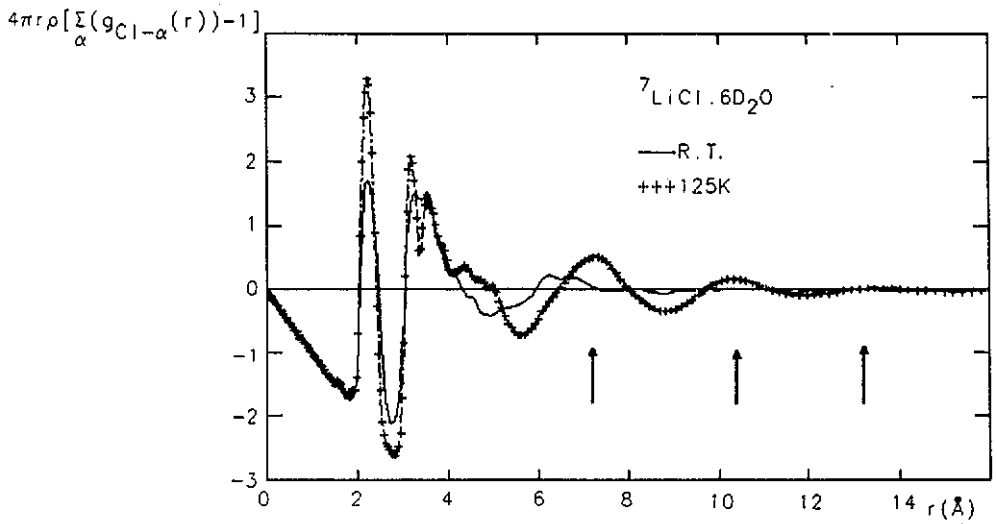

Figure 10. Pair correlation functions $4\pi r\rho(\Sigma_\alpha g_{Cl-\alpha}(r) - 1)$: +++, at 125 K; and ———, at RT.

In figure 10 we display $r(\Delta g(r) - 1)$ which allows us to make a very sensitive comparison of the chlorine–water correlations in the glassy and liquid states.

The long-range correlations extending to 14 Å in the glass disappear at about 8 Å in the liquid. This corresponds to a difference of about three shells of water molecules. In the liquid and in the glass the first coordination shell has the same characteristic, Cl–D_1, Cl–O and Cl–D_2 distances are equal, as well as the hydration number ($n_{Cl} = 5.4$) determined from the running integration number up to r_{m1}: the well defined minima at 2.675 Å. The n_{Cl-O} coordination number integrated up to $r = 3.8$ Å has nearly the same value $n_{Cl-O} = 5.7$. We take $r = 4$ Å as the spatial extent of the chlorine hydration shell.

In the range 4–5 Å, correlations appear in the glass that are smeared out in the liquid; they could be related to indirect correlations between Cl^-Cl^- and Cl^-Li^+ through water molecules (see the results of MD simulation). In the glass, the structural modulation extending to 14 Å can be taken as an estimate for the correlation length. We note that the direct ion pairing Li^+ Cl^- at around 2.8 Å is excluded at this concentration.

If we consider the D_2O intramolecular distance (O–D = 0.97 Å, D–D = 1.57 Å) and the hydration shell Cl–D and Cl–O values, we conclude that D_1, O and Cl atoms are positioned completely linearly, the D_2 atoms also being very well localized in the vitreous state in which the water molecule motion is significantly reduced compared with the liquid state case, there is a fundamental change within the hydration shell around the chlorine ion, although the mean distances and hydration number do not change. This localization enhances the orientational correlations between neighbouring molecules and increases the spatial correlation length, thus contributing to the noticeable changes in the characteristics of the first-difference structure factors (see figure 8). As in the pure water case [19] we observe shorter distances for the correlations away from the first shell in the liquid state as compared with the glassy state: they appear, respectively, at 6 Å and 7 Å in liquid and glassy $LiCl \cdot 6D_2O$, and at 3.5 Å and 4.5 Å in water and amorphous ice.

The observed hydration number is less than six, even at this concentration where the ratio $D_2O/LiCl$ is six. This is observed for most solutions containing chlorine ions, at

Table 7. Structural information obtained by various authors for the system $LiCl \cdot RD_2O$, from scattering experiments (XR or N) and molecular dynamic simulation (MD). All data are at RT. n: is the coordination number. In addition, the ratio of the peak intensities corresponding to direct versus indirect pairing is given in parentheses.

			Lithium correlations					Chlorine correlations					
Authors	$R = \frac{\text{mole water}}{\text{mole of salt}}$	Technique	Li–O (Å)	Li–D (Å)	n	Direct ion pairing (Å)	Indirect ion pairing via water molecule (Å)	Cl–D (Å)	Cl–O (Å)	n	$Cl–D_2$ (Å)	Direct ion pairing (Å)	Indirect ion pairing via water molecule (Å)
Narten *et al* 1973 [22]													
Bristol Group	14	N	1.95	2.55	5.5			2.25	3.34	5.9			
1980 [23, 24]	5	(isotopic	1.95	2.50	3			2.22	3.29	5.3			
Bristol Group 1985 [15]	3.35	substitution)	1.95	2.31	2.3			2.24	3.25	4.4	3.56	3.75	6.1
Okada *et al* 1983 [25]	4	XR, N (total), MD											
Bopp *et al* 1985 [17]	4	MD	2	2.70	5.2	2.8	4.5 (small)	2.25	3.20	6.3			4.9
Ichikawa *et al* 1984 [26]	2	N (spallation) isotopic substitution on Li	1.95	2.31	2.3	2.76	3.28 (1/1.5)	2					
Tanaka *et al* 1987 [21]	4	MD	2	2.7		2.8	4.8 1/10	2.2	3.2				4.9
	3	MD (XR)	<2	<2.7	5	2.8	4.5 (1/1)	<2.2	3.2				4.5

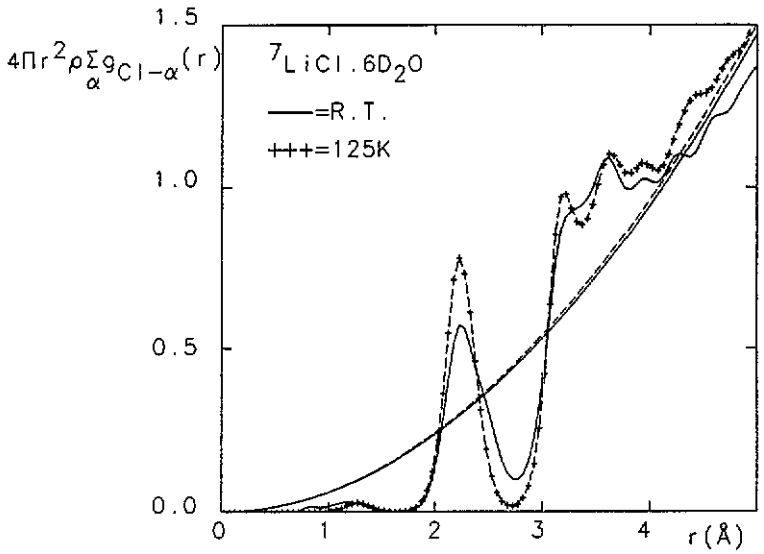

Figure 11. Radial pair correlation function $4\pi r^2 l \Sigma_\alpha g_{Cl-\alpha}(r)$: +++, at 125 K; and ———, at RT.

least up to $R = 4$. It is allegedly related to the efficiency of some dissociative mechanism [20]. The fact that, even in the vitreous state where the chlorine hydration is expected to be quite stable, the well defined local order persists with coordination number less than six brings the dissociative mechanism into doubt. But if we notice that the first stable hydrate near $R = 6$ is the pentahydrate, which exhibits a diffraction spectrum typically similar to that of a lamellar compound [2, 3], we might expect some distortion of the water molecule arrangement around chlorine for coordination six, preluding the stratification for $R = 5$.

We have summarized all the structural information obtained for the system $LiCl \cdot R D_2O$ in table 7. Inspection of the out-of equilibrium phase diagram [3] shows that RT is not an equivalent temperature for all concentrations. However, given the self-similarity of the structural behaviour in the liquid state for salt-rich concentrations, we do not expect a large temperature dependence of the structural characteristics, as long as we remain above peritectic lines [5].

Table 8. Summary of our data obtained for $R = 6$ at RT and at 125 K.

Temperature	R	Technique	Chlorine correlations					
			Cl–D (Å)	Cl–O (Å)	n	Cl–D_2 (Å)	Direct ion pairing (Å)	Indirect ion pairing via water molecule (Å)
RT	6	N	2.225	3.2	5.4	3.625	—	—
125 K	6	N	2.225	3.175	5.4	3.625	—	⟨4–5⟩

Our results are in agreement with the experimental results obtained by the Bristol group for the composition of the pentahydrate. They also agree with the results obtained by the molecular dynamics simulations of Bopp and co-workers [17] and Tanaka and co-workers [21] for the composition $R = 4$. The running number nCl–H obtained by Bopp and coworkers [17] is 5.2 at $r = 2.63$ Å and 6.3 at $r = 2.92$ Å, which compares well with the value obtained at the minimum of the function where the solvation number around Cl^- is near 5.4.

Therefore we can consider that, at RT, for the hydration $4 < R < 6$, the chlorine–water distribution does not present large variations, at least for the first hydration shell. The differences in R appear due to indirect pairing via water molecules, this pairing not being present in the liquid state at the composition $R = 6$.

Its agreement with experiment supports the improved central force model used for water, ion–water, and ion–ion interaction simulations, at least at RT.

5. Conclusion

In conclusion, we have pointed out the value of analyzing the structure of an electrolyte in the glassy state with pulsed neutron diffraction. This work will be completed by the determination of the correlations between Li^+ and D_2O in the liquid and glassy states. Given the well defined ordering detected at low temperatures we expect to be able to describe, at the atomic level, the structural changes accompanying the slow and irreversible configurational disorder appearing at the glass transition [2, 5].

Acknowledgments

We would like to thank RAL for giving us access to the LAD spectrometer at ISIS, our thanks extending to S Howells who kindly provided us with good working conditions. We also appreciate the help and collaboration of M C Bellissent who introduced us to the use of the 7C2 spectrometer at the ORPHEE reactor. Neither do we forget the valued support of the Bristol group of G W Neilson who supplied us with the sample prepared by Phil Gullidge. Finally we thank P Chieux for collaboration and helpful discussions of the data analysis and results.

References

[1] Angell C A and Sare E J 1970 *J. Chem. Phys.* **52** 1058
[2] Carmona P 1989 *Thèses* Université de Lyon
[3] Elarby-Aouizerat A, Jal J F, Chieux P, Letoffé J M, Claudy P and Dupuy J 1988 *J. Non-Cryst. Solids* **104** 203
[4] Carmona P, Aouizerat-Elarby A, Jal J F, Dupuy J, Letoffé J M, Claudy P, Bellissent-Funel M C and Chieux P 1987 *J. Non-Crystalline Solids* **95–96** 1009
[5] Dupuy J, Jal J F, Carmona P, Aouizerat-Elarby A and Chieux P 1990 *Relaxation in Complex Systems and Related Topics* (NATO ASI Series B, vol 222) ed I A Campbell and C Giovannella (New York: Plenum) p 175
[6] Elarby-Aouizerat A 1988 *Thèse d'État* Université de Lyon
[7] Soper A K and Silver R W 1982 *Phys. Rev. Lett.* **49** 471
[8] Franck H S and Wen W Y 1957 *Discuss. Faraday Soc.* **24** 133
[9] Dupuy J, Elarby-Aouizerat A, Jal J F, Chieux P, Claudy P and Letoffé J M 1984 *Rev. Stazione Sperimentale Vetro* **5** 63

[10] Koester L and Rauch H 1983 *IA EA Report No 2517*/RB, 2nd edn
[11] Soper A K, Howells W S and Hannor A C 1989 R.A.L. 89.046 (Atlas)
[12] Fornazero J, El Hachadi A and J Dupuy in preparation
[13] Soper A K 1991 *Proc. J. Chem. Phys. workshop on Neutron Scattering Data Analysis (Rutherford Appleton Laboratory, 1990)* (Bristol: IOP Publishing) at press
[14] Soper A K 1990 private communication
[15] Copestake A P, Neilson G W and Enderby J E 1985 *J. Phys. C: Solid State Phys.* **18** 4211
[16] Page D I 1983 *Water: a Comprehensive Treatise* vol 1, 4th edn ed F Franks p 333 (New York: Plenum)
[17] Bopp Ph, Okada I, Ohtaki H and Heinzinger K 1985 *Z Natursf.* a **40** 116
[18] Soper A K, Neilson G W, Enderby J E and Howe R A 1977 *J. Phys. C: Solid State Phys.* **10** 1793
[19] Bellissent M C, Bosio J and Teixera J 1987 *J. Chem. Phys.* **87** 2231
[20] Enderby J E, Cummings S, Herdman S J, Neilson G W, Salmon P S and Skipper N 1987 *J. Phys. Chem.* **91** 5851
[21] Tanaka K, Ogita N, Tamura Y, Okada I, Ohtaki H, Palinkas G, Spohr E and Heinzinger K 1987 *Z. Naturf.* **420** 29
[22] Narten A H, Vaslow F and Levy H A 1973 *J. Chem. Phys.* **58** 5017
[23] Newsome J R, Neilson G W and Enderby J E 1980 *J. Phys. C: Solid State Phys.* **13** L923
[24] Newsome J R 1981 *Thesis* University of Bristol
[25] Okada I, Kitsuno Y, Lee H G and Ohtaki H 1983 *Ions and Molecules in Solutions* ed N Tanaka, H Ohtahi and R Tamamushe (Amsterdam: Elsevier) 81
[26] Ichikawa K, Kameda Y, Matsumoto T and Misawa M 1984 *J. Phys. C: Solid State Phys.* **17** L725